The University of Bradford Institutional Repository

http://bradscholars.brad.ac.uk

SHEAR CAPACITY OF MONOLITHIC CONCRETE JOINTS WITHOUT TRANSVERSE REINFORCEMENT

Keun-Hyeok Yang[a], Jae-Il Sim[b] and Ashraf F. Ashour[c]

[a] *Corresponding author, Department of Architectural Engineering, Mokpo National University, Mokpo, Jeonnam, South Korea.*

[b] *Department of Architectural Engineering, Mokpo National University, Mokpo, Jeonnam, South Korea.*

[c] *EDT 1, School of Engineering, Design and Technology, University of Bradford, Bradford, BD7 1DP, UK.*

Biography: Keun-Hyeok Yang is an assistant professor at Mokpo National University, South Korea. He received his MSc and PhD degrees from Chungang University, Korea. His research interests include ductility, strengthening, plasticity and shear of reinforced concrete structures.

Jae-Il Sim is a doctoral student at Mokpo National University, South Korea. His research interests include shear and plasticity of reinforced eco-friendly concrete structures.

Ashraf F. Ashour is the director of civil engineering at the University of Bradford, UK. He obtained his BSc and MSc degrees from Mansoura University, Egypt and his PhD from Cambridge University, UK. His research interests include shear, plasticity and optimization of reinforced concrete and masonry structures.

ABSTRACT

A mechanism analysis based on upper-bound theorem of concrete plasticity for monolithic concrete joints without transverse reinforcement is presented. Concrete is modelled as a rigid perfectly plastic material obeying a modified Coulomb failure criteria. Existing stress-strain relationships of concrete in compression and tension are comprehensively modified using the crack band theory to consider the effect of concrete type and maximum aggregate size on the profile of the stress-strain curves. Simple equations for the effectiveness factor for compression, ratio of effective tensile to compressive strengths and angle of concrete friction are then developed using the modified stress-strain relationships of concrete. In addition, 12 push-off specimens made of all-lightweight, sand-lightweight and normal weight concrete having maximum aggregate size between 4 and 19 mm were physically tested. Test results and mechanism analysis clearly showed that the shear capacity of monolithic concrete joints increased with the increase of the maximum aggregate size and dry density of concrete. The mean and standard deviation of the ratio between experimentally measured and predicted by the mechanism analysis shear capacities are 1.27 and 0.18, respectively, showing a slightly closer prediction and less variation than Vecchio and Collins' equation, regardless of the concrete type and maximum aggregate size.

Keywords: monolithic concrete joints, shear capacity, mechanism analysis, lightweight concrete, aggregate size.

INTRODUCTION

The monolithic concrete joints commonly occur at the interface between columns and corbels, shear walls and columns, and shear keys. Their structural performance is mainly governed by shear transferred across the shear plane between the two members due to aggregate interlock or shear friction [1, 2]. Mattock and Hawkins [3] concluded that the resistance of lightweight concrete shear

2

planes to slip along shear cracks is less than that of normal weight concrete, as the crack face of lightweight concrete is smoother than that of normal weight concrete. Other experimental data [4] also showed that shear cracks in normal strength, normal weight aggregates concrete propagate through cement matrix around aggregate particles, while these in lightweight aggregate concrete mainly penetrate through coarse aggregate particles. As a result, Sherwood et al. [5] pointed out that shear transferred by aggregate interlock would be negligible in lightweight concrete. However, experimental investigations to evaluate the reduced shear capacity of lightweight concrete joints are very scarce.

ACI 318-08 provision [6] recommended the shear friction model [7] for concrete joint design and also specified a modification factor for lightweight concrete, based on experimental data of simply supported beams [8], to account for the reduced shear strength, friction properties, and splitting resistance of lightweight concrete compared with normal weight concrete of the same compressive strength. Yang et al. [4] concluded that the modification factor for lightweight concrete continuous beams in ACI 318-08 is potentially un-conservative and, as a result, proposed the use of maximum aggregate size and dry density of concrete in the modification factor calculation. In particular, ACI 318-08 provision and the empirical equation proposed by Mattock [9] neglect the concrete shear capacity; which can result in transverse reinforcement congestion at concrete joints. Therefore, a rational approach would be required to explain the shear transfer mechanism in concrete joints, considering the effect of strength and size of aggregates.

In the present study, a mechanism analysis is developed using the upper-bound theorem of concrete plasticity in order to predict the shear transfer capacity of concrete in monolithic joints. 12 push-off specimens without transverse reinforcement were also tested according to the variation of the concrete type and maximum aggregate size. The measured shear capacity of the concrete joints tested is compared with the predictions obtained from the mechanism analysis and empirical formulas proposed by Vecchio and Collins [10].

3

SIGNIFICANCE OF RESEARCH

Although concrete cohesion and aggregate interlock along the shear plane of monolithic concrete joints have a significant influence on the concrete shear capacity, ACI 318-08 provision and empirical formulas proposed by Mattock based on shear friction theory neglect the concrete contribution along the shear plane of such joints. A mechanism analysis is developed to identify the shear transfer of concrete in monolithic joints as the inclusion of concrete shear capacity in joint design would produce a proper arrangement of shear-friction reinforcement. Test results and mechanism analysis showed that the shear capacity of the shear plane of concrete joints increased with the increase of maximum aggregate size.

REVIEW OF EXISTING MODELS

Currently available models to evaluate the shear capacity of concrete joints are generally based on the shear friction theory [6] or empirical regression analysis of experimental data [9, 10]. Although, more sophisticated models [11, 12] were also developed, they are complicated and tedious to follow. Existing simple formulas for estimating the shear capacity of concrete joints are summarized below.

ACI 318-08 [6]

ACI 318-08 specified the shear capacity V_n of monolithic concrete joints without axial force based on the shear friction theory as:

$$V_n = A_f f_y \left(1.4\lambda \sin\alpha_f + \cos\alpha_f \right) \tag{1}$$

where A_f and f_y = total area and yield strength of transverse reinforcement across the shear plane, respectively, α_f = angle between transverse reinforcement and shear plane, and λ = modification factor recommended to be 0.75 for all-lightweight concrete, 0.85 for sand-lightweight concrete and 1.0 for normal weight concrete. When the average splitting tensile strength f_{sp} is specified, the

4

modification factor is alternatively obtained from $\lambda = f_{sp}/\left(0.56\sqrt{f_c^{'}}\right) \leq 1.0$. As Eq. (1) becomes un-

conservative for few cases of normal weight concrete having concrete strength above 28 MPa or

over-reinforced shear plane joints [3, 9], the code specifies that the shear capacity of monolithic

concrete joints shall not exceed an upper limit $\left(V_n\right)_{\max}$ (in N) as given below:

$$\left(V_n\right)_{\max} = \text{Min of } \{0.2f_c^{'}A_c\}, \; \{\left(3.3+0.08f_c^{'}\right)A_c\} \text{ or } \{11A_c\} \qquad \text{for normal weight concrete} \qquad \text{(2 a)}$$

$$\left(V_n\right)_{\max} = \text{Min of } \{0.2f_c^{'}A_c\} \text{ or } \{5.5A_c\} \qquad \text{for lightweight concrete} \qquad \text{(2 b)}$$

where $f_c^{'}$ = concrete compressive strength (in MPa), and A_c = area of concrete section resisting

shear (in mm^2). Eq. (2) indicates that the upper limit is governed by $0.2f_c^{'}A_c$ when compressive

strength is less than 28 MPa, regardless of concrete type, while it is governed by $\left(3.3+0.08f_c^{'}\right)A_c$

for normal weight concrete when $f_c^{'}$ is between 28 MPa and 100 MPa. Eqs (1) and (2) also imply

that there is no concrete joint capacity gain for any increase of the transverse reinforcement index

$\dfrac{\rho_f f_y}{f_c^{'}}$ beyond $\dfrac{0.2}{1.4\lambda\sin\alpha_f + \cos\alpha_f}$ for concrete strength less than 28 MPa, where $\rho_f\left(=\dfrac{A_f}{A_c}\right)=$

transverse reinforcement ratio. The shear friction model ignores concrete cohesion and assumes that

the applied shear force is entirely transferred by friction, as a result, no shear transfer capacity of

concrete along shear plane is considered. This indicates that ACI 318-08 would be too conservative

for high-strength concrete joints, as pointed out by Mattock [9].

Mattock [9]

Mattock [3] proposed that cohesion together with friction should be considered to rationally

evaluate the shear capacity of concrete joints having transverse reinforcement perpendicular to the

shear plane. Based on the basic equation form proposed in 1972, Mattock [9] empirically developed

the shear capacity V_n of monolithic concrete joints without axial force as below:

$$V_n = K_1 A_c + 0.8 A_{fv} f_{yv} \leq \text{Min. of } K_2 f_c' A_c \text{ or } K_3 A_c \qquad \text{for } A_{fv} f_{yv} \geq K_1 A_c / 1.45 \qquad (3.a)$$

$$V_n = 2.25(A_{fv} f_{yv}) \qquad \text{for } A_{fv} f_{yv} < K_1 A_c / 1.45 \qquad (3.b)$$

where A_{fv} and f_{yv} = total area and yield strength of the transverse reinforcement perpendicular to the shear plane, respectively, K_1, K_2, and K_3 = empirical constants determined from regression analysis of 199 push-off test data with f_c' ranging from 17 MPa to 100 MPa. The constants K_1, K_2, and K_3 are $0.1 f_c' (\leq 5.5 \, \text{MPa})$, 0.3, and 16.6 MPa, respectively, for normal weight concrete, 1.38, 0.2 and 8.3 MPa, respectively, for all-lightweight concrete, and 1.73, 0.2 and 8.3 MPa, respectively, for sand-lightweight concrete. Mattock's equation also ignores the shear transfer contribution of concrete when $\rho_{fv} f_{yv} < K_1 / 1.45$, where $\rho_{fv} \left(= \dfrac{A_{fv}}{A_c} \right)$ = ratio of transverse reinforcement perpendicular to the shear plane.

Vecchio and Collins [10]

Walraven [12] concluded that the shear force transferred along shear crack is significantly dependent on the crack width w and maximum aggregate size d_a based on a comprehensive testing of 88 push-off concrete specimens. Vecchio and Collins fitted the test data carried out by Walraven and proposed a shear capacity formula considering only concrete contribution as follows:

$$V_n = \frac{0.18\sqrt{f_c'}}{0.3 + \left(\dfrac{24 w_c}{d_a + 16} \right)} A_c \qquad (4)$$

where the maximum crack width w_c at failure of concrete element and maximum aggregate size d_a are in mm. The maximum crack width w_c can be obtained from:

$$w_c = \varepsilon_1 s_x \qquad (5)$$

where ε_1 = principal tensile strain along the shear plane, and s_x = spacing of cracks. For a shear plane under pure shear stress, ε_1 can be obtained from $\gamma_{xy}/2$, where γ_{xy} = shear strain along the shear plane. As the failure crack of monolithic concrete joint is locally formed along the shear plane [2, 3], the spacing s_x of cracks can be replaced by the crack band width h_c [13].

MECHANISM ANALYSIS

Failure mechanism

Figure 1 shows a typical failure plane of a monolithic concrete joint under shear [2, 3]. At failure, the concrete joint can be idealized as composed of two rigid blocks separated by a failure surface. One rigid block has two translational and rotational displacement components relative to the other rigid block. Therefore, one rigid block can be assumed to be rotating about an instantaneous center (IC) as shown in Fig. 1. For the idealized failure mechanism, the lateral (out of plane) strains are prevented. Hence, the concrete joint at failure can be regarded as a plane strain problem [14].

Upper bound solution

The upper bound analysis uses the energy principle to calculate the shear capacity for the kinematically admissible failure mechanism explained above. The external work W_E of the vertical applied load V at failure is:

$$W_E = V\omega X_{ic} \tag{6}$$

where ω = relative rotational displacement of rigid block *I* to rigid block *II* about IC, and X_{ic} = horizontal coordinate of IC as shown in Fig. 1.

For a plane strain problem, the internal energy W_I dissipated in concrete along the hyperbolic failure surface is estimated from the following general formula [14]:

$$W_I = \frac{1}{2} f_c^* \delta [l - m \sin \alpha] A_c \tag{7}$$

7

where $l = 1 - 2 \dfrac{f_t^*}{f_c^*} \dfrac{\sin \varphi}{1 - \sin \varphi}$, $m = 1 - 2 \dfrac{f_t^*}{f_c^*} \dfrac{1}{1 - \sin \varphi}$, f_c^* and $f_t^* =$ effective compressive and tensile

strengths of concrete, respectively, $\alpha =$ angle between the relative displacement δ at the chord

midpoint and the failure plane chord, and $\varphi =$ angle of concrete friction. The relative displacement

δ can be also written as $\omega \cdot \left(\dfrac{X_{ic}}{\cos \alpha} \right)$, as presented in Fig. 1.

Equating the total internal energy dissipated in concrete to the external work done, the shear

capacity of monolithic concrete joints without transverse reinforcement can be derived in the

following form:

$$V_n = \frac{1}{2} f_c^* \frac{1}{\cos \alpha} [l - m \sin \alpha] A_c \tag{8}$$

According to the upper-bound theorem, the collapse occurs at the least strength. The shear

capacity of concrete joints without transverse reinforcement varies with the change in the angle α,

as given in the above Eq. (8). Hence, the determination of the minimum shear capacity could be

achieved by considering the differential equation, $\dfrac{\partial V_n}{\partial \alpha} = 0$, which gives:

$$\alpha = 2 \tan^{-1} \left(\frac{x}{\sqrt{x^2 + y^2} + y} \right) \tag{9}$$

where $x = m / l$, $y = \sqrt{l^2 - m^2} / l$.

Modelling of concrete

Concrete can be regarded as a rigid perfectly plastic material obeying a modified Coulomb failure

criteria with effective compressive f_c^* and tensile f_t^* strengths [14]. As concrete is not a perfectly

plastic material but a typical brittle material, effectiveness factor for compression can be determined

from equating the area of the rigid-perfectly plastic stress-strain curve to that of the actual stress-

strain curve [17], as shown in Fig. 2. Therefore, the effectiveness factor v_c for concrete in compression can be defined as below [15]:

$$v_c = \frac{f_c^*}{f_c'} = \int_0^1 \left(\frac{\sigma_c}{f_c'} \right) d \left(\frac{\varepsilon_c}{\varepsilon_u} \right)$$ (10)

where σ_c = compressive stress corresponding to compressive strain ε_c, and ε_u = ultimate strain in compression.

Similarly, the effectiveness factor v_t for concrete in tension can be defined as below:

$$v_t = \frac{f_t^*}{f_t} = \int_0^1 \left(\frac{\sigma_t}{f_t} \right) d \left(\frac{\varepsilon_t}{\varepsilon_{tu}} \right)$$ (11)

where σ_t = tensile stress corresponding to tensile strain of ε_t, and ε_{tu} = ultimate tensile strain.

Stress-strain relationships of concrete

The shape of concrete compressive stress-strain curve is strongly affected by the concrete strength and elastic modulus of aggregates [1]. For instance, a closer to linear ascending branch and steeper descending branch are observed in high strength concrete than normal strength concrete [1]. In addition, a lower elastic modulus and more brittle descending branch are observed in lightweight concrete than normal weight concrete of the same compressive strength, as depicted in Fig. 3. CEB-FIP [16] also recommends that stresses below $0.5 f_c'$ on the descending branch would be neglected. The compressive stress-strain relationship generalized by Thorenfeldt et al. [17] is modified to accommodate the above mentioned characteristics as follows:

$$\sigma_c = \frac{n(\varepsilon_c / \varepsilon_0)}{n - 1 + (\varepsilon_c / \varepsilon_0)^{nk}} f_c'$$ (12)

where n = a curve-fitting parameter, $\varepsilon_0 \left(= \frac{f_c'}{E_c} \left(\frac{n}{n-1} \right) \right)$ = strain corresponding to the peak stress f_c', E_c = concrete elastic modulus and k = factor controlling the slopes of the ascending and descending

branches of the stress-strain curve. The modulus of elasticity of concrete is assumed to follow the equation specified in ACI 318-08 below:

$$E_c = 0.043\left(\rho^{1.5}\right)\sqrt{f_c'} \quad \text{(MPa)} \tag{13}$$

where ρ = dry density of concrete (in kg/m^3). To reflect the lower elastic modulus and more brittle failure of lightweight concrete, n is associated with a correction factor η_E for lightweight concrete specified in EC 2 [18] as below:

$$n = \left\{0.8 + \frac{f_c'}{17.2}\right\} \times \frac{1}{\eta_E} \tag{13}$$

$$\eta_E = \left(\frac{\rho}{2200}\right)^2 \leq 1.0 \tag{14}$$

The factor k in Eq. (12) is obtained from

$$k = 1.0 \qquad \text{for } \varepsilon_c / \varepsilon_0 \leq 1.0 \tag{15 a}$$

$$k = 0.67 + f_c' / 62 \geq 1.0 \qquad \text{for } \varepsilon_c / \varepsilon_0 > 1.0 \tag{15 b}$$

The behavior of concrete in tension without a crack is commonly assumed to be linear elastic, while that after cracking is significantly dependent on the crack opening size. According to the cohesive crack model [13], concrete can transfer tensile stresses until the crack width reaches a certain limit. This implies that the tensile strength drops to zero when the crack is completely formed, as a result, ε_{tu} can be assumed as the strain corresponding to $f_t = 0$, as shown in Fig. 2. The propagation of crack width is also affected by the contact area between aggregates and cement matrix [12]. Bažant and Sun [19] showed that the aggregate size factor $\eta_a = d_a / c_0$ should be considered to represent the aggregate interlock contribution to the shear stress transfer along diagonal tensile cracks, where $c_0 (= 25\,\text{mm}) =$ reference size of aggregate. This indicates that tensile stresses at an arbitrary crack opening decrease with the decrease of the maximum aggregate size. In the present study, based on the function of crack opening derived experimentally by Hordijk [20]

10

modified for the effect of aggregate size, the tensile stress-strain relationship of concrete is represented in the following form (see Fig. 4):

$$\sigma_t = E_c \varepsilon_t \quad \text{for } \varepsilon_t / \varepsilon_{t0} \leq 1.0 \tag{16 a}$$

$$\sigma_t = \left\{ \left[1 + \left(c_1 \frac{\varepsilon_t}{\varepsilon_{tu}} \right)^3 \right] \exp\left(c_2 \frac{\varepsilon_t}{\varepsilon_{tu}} \right) - \frac{\varepsilon_t}{\varepsilon_{tu}} \left(1 + c_1^{\ 3} \right) \exp\left(c_2 \right) \right\} f_t \times \eta_a \quad \text{for } \varepsilon_t / \varepsilon_{t0} > 1.0 \tag{16 b}$$

where $\varepsilon_{t0} \left(= \dfrac{f_t}{E_c} \right) =$ strain corresponding to f_t, and c_1 and c_2 = 3.0 and -6.93, respectively, as empirical constants. The tensile strength of lightweight concrete is commonly lower than that of normal weight concrete of the same compressive strength [18]. Therefore, CEB-FIP equation [16] to predict the tensile strength of concrete is associated with a correction factor for reduced tensile strength of lightweight concrete specified in EC 2 [18] as follows:

$$f_t = \left[2.12 \times \ln\left(1 + f_c' / 10 \right) \right] \times \eta_1 \qquad (f_t \text{ in MPa}) \tag{17}$$

$$\eta_1 = \left(0.4 + 0.6 \rho / 2200 \right) \leq 1.0 \tag{18}$$

From the tensile stress-crack opening relationship, the ultimate tensile strain ε_{tu} corresponding to $f_t = 0$ can be calculated from:

$$\varepsilon_{tu} = \frac{w_c}{h_c} \tag{19}$$

where h_c = crack band width and w_c = crack opening at the complete release of tensile stresses, which can be obtained from $5.14 G_f / f_t$ [20], G_f = concrete fracture energy. As the concrete fracture energy identifies the amount of energy required for crack growth, fracture energy of lightweight concrete would be lower than that of normal weight concrete due to the reduced friction properties and splitting resistance. The fracture energy is significantly influenced by not only concrete strength but also various characteristics of aggregates. However, very few [16] equations for concrete fracture energy are available in the literature and, therefore, the concrete fracture energy

equations specified in CEB-FIP associated with a correction factor η_E of EC 2 are adopted in the present study as below:

$$G_f = \eta_E G_{fo}\left(f_c^{'} / f_{co}\right)^{0.7} \qquad \text{for } f_c^{'} \leq 80\,\text{MPa} \qquad (20\,\text{a})$$

$$G_f = 4.3\eta_E G_{fo} \qquad \text{for } f_c^{'} > 80\,\text{MPa} \qquad (20\,\text{b})$$

where f_{co} (= 10 MPa)= reference concrete strength, and G_{fo} = basic fracture energy (in N/mm). CEB-FIP proposes different values of G_{fo} based on the maximum aggregate size d_a of concrete. The crack band width h_c cannot be determined from fracture tests in which a single crack is formed, yet it can be identified as a zone where the crack is forced to be distributed [13].

From a numerical calculation using the crack band model, Bažant and Planas [13] showed that the crack band width can be simply expressed as follows:

$$h_c = \frac{l_{ch}}{\left(1 - E_c / E_t\right)} \qquad (21)$$

where $l_{ch}\left(= \dfrac{E_c G_f}{f_t^{2}}\right)$ = characteristic length corresponding to half the length of a concrete specimen subjected to axial tension in which just enough elastic strain energy is stored to create one complete fracture surface, and E_t = softening modulus at peak tensile strength, which can be evaluated from Eq. (16b).

Effectiveness factor for compression and effective strength ratio

The effectiveness factor v_c of concrete in compression is significantly affected by the compressive strength and dry density of concrete, yet independent of the maximum aggregate size, as presented in Eq. (12) and Fig. 3. A nonlinear multiple regression (NLMR) analysis is carried out for the results obtained from Eq. (10) for v_c against concrete having $f_c^{'}$ between 20 and 80 MPa and ρ between 1200 and 2200 kg/m^3 to obtain a simple equation for v_c. Different influencing

parameters were combined and tuned repeatedly by trial and error approach using SPSS software [21] until a relatively higher correlation coefficient R^2 (=0.97) is achieved. Overall, as plotted in Fig. 5, v_c can be expressed in the following form:

$$v_c = 0.8\left[f_c^{'}/(f_{co} \times \eta_E)\right]^{-0.12} \tag{22}$$

On the other hand, the effective strength ratio f_t^{*}/f_c^{*} required for the estimation of parameters l and m is dependent on $f_c^{'}$ and ρ as well as d_a, as the effectiveness factor v_t for concrete in tension is significantly affected by these parameters. From a NLMR analysis of the results obtained from Eqs. (10) and (11) against concrete having $f_c^{'}$ between 20 and 80 MPa, ρ between 1200 and 2200 kg/m^3 and d_a between 4 and 25 mm, f_t^{*}/f_c^{*} plotted in Fig. 6 can be simply written in the following form:

$$\frac{f_t^{*}}{f_c^{*}} = 0.03\left[\frac{f_c^{'}(c_0/d_a)^{0.6}}{f_{co} \times \eta_E^{0.2}}\right]^{-0.4} \tag{23}$$

Angle of concrete friction

As plotted in Fig. 7, the condition for sliding failure of a modified Coulomb material under pure shear stress [14] is

$$\frac{1}{2}(\sigma_1 - \sigma_3) = c \cdot \cos\varphi \tag{23}$$

where σ_1 and σ_3 = principal stresses, which equal to $\pm\tau$ under pure shear stress τ, and c = cohesion of concrete. The cohesion of concrete with sliding failure is expressed as $f_c^{*}/2\sqrt{k}$ [14], where the quantity k is defined by $\dfrac{1+\sin\varphi}{1-\sin\varphi}$. Hence, the shear stress in the shear plane of concrete joint can be expressed as follows:

$$\tau = \frac{V}{A_c} = \frac{f_c^{*}\cos\varphi}{2\sqrt{k}} \tag{24}$$

13

At failure of concrete joints, shear stresses obtained from Eq. (24) should be the same as that calculated from Eq. (8) and consequently the below condition is obtained:

$$\frac{\cos\varphi}{\sqrt{k}} = \frac{l - m\sin\alpha}{\cos\alpha} \tag{25}$$

The angle φ of concrete friction is plotted against f_t^* / f_c^* in Fig. 8. Therefore, φ can be expressed as a function of f_t^* / f_c^* using a simple linear regression analysis as given below.

$$\varphi = 80\exp\left(-10.7\frac{f_t^*}{f_c^*}\right) \tag{26}$$

EXPERIMENTAL VERIFICATION

Details of test specimens

Twelve push-off specimens made of all-lightweight, sand-lightweight and normal weight concrete were tested under pure shear as shown in Fig. 9. The maximum aggregate size d_a varied from 4 mm to 19 mm in each concrete type group. All specimens tested had the same geometrical dimensions. The length and depth of test zone of specimens were 200 mm and 120 mm, respectively, producing a section area A_c of shear plane of 24000 mm^2. All test specimens had no transverse reinforcement. The concrete mix proportions of each specimen are presented in Table 1. The specimen notation listed in Table 1 identifies the type of concrete ("A" for all-lightweight concrete, "S" for sand-lightweight concrete and "N" for normal weight concrete) and the maximum aggregate size, respectively. For example, A8 is an all-lightweight concrete specimen having a maximum aggregate size of 8mm.

All push-off specimens were tested to failure under concentric load acting as a pure shear in the shear plane of the test zone as shown in Fig. 9. The top and bottom stubs of the test specimens were strengthened with carbon fiber sheets to prevent bearing failure at the interfaces between the test

zone and both stubs. The shear strain in the shear plane was measured by a strain rosette consisted of three 75 mm electrical resistance (ERS) strain gages, as shown in Fig. 9.

Test results

All test specimens failed along the shear plane as idealized in the mechanism analysis presented earlier in the paper. The shear stiffness of push-off specimens increased with the increase of d_a, regardless of the type of concrete as shown in Fig. 10. In addition, slightly higher shear stiffness developed in normal weight concrete (NWC) specimens than lightweight concrete (LWC) specimens, as depicted in Fig. 10. Table 2 presents the shear capacity V_n (kN), shear strain γ_{xy} and normalized shear stresses $\dfrac{\tau_n}{\sqrt{f_c^{'}}}$ of test specimens. The normalized shear capacity $\tau_n / \sqrt{f_c^{'}}$ of the shear plane is also plotted against the maximum aggregate size in Fig. 11. The normalized shear capacity $\tau_n / \sqrt{f_c^{'}}$ of the shear plane is also significantly affected by the type of concrete and d_a, though similar values of $\tau_n / \sqrt{f_c^{'}}$ were observed for specimens A-4, S-4, and N-4 whose concrete had d_a of 4 mm as shown in Fig. 11. The normalized shear capacity is commonly increased with the increase of d_a, showing the highest increasing rate in NWC specimens and similar increasing rate in ALWC and SLWC specimens, as given in Table 2 and Fig. 11. At the same d_a, $\tau_n / \sqrt{f_c^{'}}$ of NWC specimens was higher than that of SLWC specimen which, in turn, is higher than that of ALWC specimen. The measured shear capacity of all specimens was much lower than the maximum values obtained from Eq. (2) specified in ACI 318-08, as given in Table 2, as no transverse reinforcement was provided in the test specimens.

Comparisons of measured and predicted shear capacities

The shear capacity of push-off specimens tested was predicted using the extended version of Vecchio and Collins' method (Eqs. 4 and 5) and mechanism analysis developed in the present study

as listed in Table 2. As the equations proposed by ACI 318-08 and Mattock neglect the concrete shear capacity of monolithic joint without transverse reinforcement, no predictions by these equations are presented in Table 2. The shear capacity predicted from Vecchio and Collins' equation is minimally affected by the maximum aggregate size and dry density of concrete as listed in Table 2. The means and standard deviations of the ratio between measured and predicted by Vecchio and Collins' equation shear capacities are 0.76 and 0.14 for ALWC, 0.84 and 0.11 for SLWC and 1.07 and 0.35 for NWC specimens, respectively, whereas the corresponding statistical parameters of the ratio between measured and predicted by the mechanism analysis shear capacities are 1.22 and 0.13 for ALWC, 1.25 and 0.15 for SLWC and 1.35 and 0.23 for NWC specimens, respectively. Vecchio and Collins' equation generally overestimates the shear capacity of monolithic concrete joints for $d_a \leq 13$ mm. On the other hand, the predictions obtained from the mechanism analysis are generally lower than the measured shear capacities. However, the deviations of the ratio between measured and predicted by the mechanism analysis shear capacities were slightly smaller than these from Vecchio and Collins' equation, regardless of concrete type and maximum aggregate size d_a. Therefore, the proposed mechanism analysis can be conservatively applicable for predicting the concrete shear capacity of monolithic concrete joints without transverse reinforcement.

CONCLUSIONS

A mechanism analysis based on upper-bound theorem is developed to predict the concrete shear capacity of monolithic concrete joints without transverse reinforcement. The concrete is identified as a rigid perfectly plastic material obeying a modified Coulomb failure criteria. Simple equations for the effectiveness factor for compression, ratio of effective strength and angle of concrete friction are proposed using modified stress-strain relationships of concrete in compression and tension. In

addition, 12 push-off specimens made of all-lightweight, sand-lightweight and normal weight concrete having maximum aggregate sizes of 4, 8, 13 and 19mm, without transverse reinforcement were tested. The shear capacity measured in the failure shear plane of test specimens is compared with predictions obtained from the proposed mechanism analysis and extended version of Vecchio and Collins' equation. Based on the analytical solution and test results, the following conclusions may be drawn:

1. The normalized shear capacity of the shear plane of push-off specimens is commonly increased with the increase of maximum aggregate size. The normal weight concrete specimens exhibited the largest increasing rate of the normalized shear capacity, whereas all-lightweight and sand-lightweight concrete specimens had a similar increasing rate of the normalized shear capacity.

2. The equation proposed by Vecchio and Collins generally overestimates the shear capacity of monolithic concrete joints having maximum aggregate size above 13 mm. In particular, Vecchio and Collins' equation minimally considers the effect of maximum aggregate size and dry density of concrete on the shear transfer capacity of concrete.

3. The mechanism analysis predictions are generally lower than the measured shear capacity and, therefore, can be conservatively applicable for the prediction of the concrete shear capacity of monolithic concrete joints.

ACKNOWLEDGMENTS

NOTATION

A_c = section area of shear plane

A_f = area of transverse reinforcement across shear plane

d_a = maximum size of aggregate

c = cohesion of concrete

c_0 = reference aggregate size (=25 mm)

$f_c^{'}$ = concrete compressive strength

f_{co} = reference concrete compressive strength (=10 MPa)

f_c^{*} = effective compressive strength of concrete

f_t = concrete tensile strength

f_t^{*} = effective tensile strength of concrete

E_c = modulus of elasticity of concrete

E_t = softening modulus at peak tensile strength of concrete

G_f = concrete fracture energy

h_c = width of crack band

V_n = shear capacity in shear plane of concrete joint

W_E = external work done by applied load

W_I = concrete internal energy dissipated in failure surface

w_c = maximum crack width in shear plane

α = angle between the relative displacement and failure surface

α_f = angle between transverse reinforcement and shear plane

γ_{xy} = shear strain in shear plane

δ = relative displacement vector

ε_u = ultimate strain of concrete in compression

ε_{tu} = ultimate strain of concrete in tension

ν_c = effectiveness factor for concrete compressive strength

ν_t = effectiveness factor for concrete tensile strength

ρ = dry density of concreteo

ρ_f = transverse reinforcement ratio

τ = shear stress in shear plane

φ = friction angle of concrete

ω = relative rotational displacement of rigid block *I* to rigid block *II* about IC.

REFERENCES

1. MacGregor, J. G., and Wight, J. K., Reinforced Concrete: Mechanics and Design, Prentice Hall, 2005.

2. ACI-ASCE Committee 426, "The Shear Strength of Reinforced Concrete Members," Proceedings ASCE, Journal of the Structural Division, V. 99, No. ST6, 1973, pp. 1091-1187.

3. Mattock, A. H., and Hawkins, N. M., "Shear Transfer in Reinforced Concrete-Recent Research," Journal of the Prestressed Concrete Institute, V. 17, No. 2, 1972, pp. 55-75.

4. Yang, K. H., Sim, J. I., and Lee, E. T., "Effect of Aggregate Size on Shear Behavior of Lightweight Concrete Continuous Slender Beams," ACI Structural Journal, Under Review, 2009.

5. Sherwood, E. G., Bentz, E. C., and Collins, M. P., "Effect of Aggregate Size on Beam-Shear Strength of Thick Slabs," ACI Structural Journal, V. 104, No. 2, 2007, pp. 180-190.

6. ACI Committee 318, Building Code Requirements for Structural Concrete (ACI 318-08) and Commentary (ACI 318R-08), American Concrete Institute, Farmington Hills, MI, 2008. 473 pp.

7. Hofbeck, J. A., Ibrahim, I. A., and Mattock, A. H., "Shear Transfer in Reinforced Concrete," ACI Journal, Proceedings, V. 66, No. 2, 1969, pp. 119-128.

8. Ivey, D. I., and Buth, E., "Shear Capacity of Lightweight Concrete Beams," ACI Journal, Proceedings, V. 161, No. 10, 1967, pp. 634-643.

9. Mattock, A. H., "Shear Friction and High-Strength Concrete", ACI Structural Journal, V. 98, No. 1, 2001, pp. 50-59.

10. Vecchio, F. J., and Collins, M. P., "The Modified Compression Field Theory," ACI Journal, Proceedings, V. 83, No. 2, 1986, pp. 219-231.

11. Ali, M. A., and White, R. N., "Enhanced Contact Model for Shear Friction of Normal and High-Strength Concrete," ACI Structural Journal, V. 96, No. 3, 1999, pp. 348-360.

12. Walraven, J. C., "Fundamental Analysis of Aggregate Interlock," Journal of the Structural Division, ASCE, V. 107, No. ST11, 1981, pp. 2245-2271.

13. Bažant Z. P., and Planas J., *Fracture and Size Effect in Concrete and Other Quasibrittle Materials*. CRC Press, 1998.

14. Nielsen M. P. *Limit Analysis and Concrete Plasticity*, Prentice-Hall, Englewood Cliffs, 1984.

15. Exner, H., "On the effectiveness factor in plastic analysis of concrete," Plasticity in reinforced concrete (Reports of the Working Commission), International Association for Bridge and Structural Engineering, Zurich, Switzerland, 1979, pp. 35-42.

16. Comité Euro-International du Beton (CEB-FIP), "CEB-FIP Model Code 1990 for Concrete Structures," *Bulletin d'Information No. 213-214, CEB-FIP 90*, Lausanne, 1993.

17. Thorenfeldt, E., Tomaszewicz, A., and Jensen, J. J., "Mechanical properties of High Strength Concrete and Application to Design," Proceedings of the Symposium: Utilization of High-Strength Concrete, 1987, pp. 149-159.

18. The European Standard EN 1992-1-1:2004. *Eurocode 2: Design of concrete structures*, British Standards Institution, London, UK, 2004, 225 pp.

19. Bažant, Z. P., and Sun, H. H., "Size Effect in Diagonal Shear Failure: Influence of Aggregate Size and Stirrups," ACI Materials Journal, V. 84, No. 4, 1987, pp. 259-272.

20. Hordijk, D. A., "Local Approach to Fatigue of Concrete," Doctor Dissertation, Delft University of Technology, Netherlands, 1991.

21. SPSS Inc., SPSS 13.0: Regression Models, Prentice Hall, USA, 2004.

Table 1 – Concrete mix proportions

Specimen	Type of concrete	d_a (mm)	W/B	S/A	Unit weight[#] (kg/m³)					R_{sp} (%)
					W	C	SF	F	G	
A4	All-lightweight	4	0.4	-	139	348	0	1043	0	0.75
A8		8	0.36	0.4	222	548	61	320	439	0.21
A13		13	0.35		212	545	61	327	448	0.45
A19		19	0.30		173	518	58	326	447	0.50
S4	Sand-lightweight	4	0.52	-	260	495	0	1486[*]	0	0.00
S8		8	0.35	0.4	198	569		634[*]	474	0.19
S13		13	0.36		203	556		633[*]	473	0.15
S19		19	0.33		171	525		625[*]	467	0.21
N4	Normal-weight	4	0.50	-	250	502		1505[*]	0	0.00
N8		8	0.65	0.4	201	309		715[*]	1097[*]	0.20
N13		13	0.63		193	309		723[*]	1110[*]	0.13
N19		19	0.60		186	309		731[*]	1122[*]	0.13

Note: d_a = maximum size of aggregate, W/B = water-to-binder ratio by weight, S/A = fine aggregate-to-total aggregate ratio by volume, and R_{sp} = ratio of super-plasticizer to binder by weight.

\# W, C, SF, F, and G refer to water, ordinary Portland cement, silica fume, fine aggregate, and coarse aggregate, respectively.

* indicates natural normal weight aggregates.

Table 2 – Summary of test results and comparisons of measured and predicted shear capacities.

| Specimen	$f_c^{'}$ (MPa)	ρ (kg/m³)	Test results at failure			ACI 318-08	Vecchio and Collins		Mechanism analysis					$\dfrac{(V_n)_{Exp.}}{(V_n)_{Pr\,e.}}$	
			V_n (kN)	γ_{xy} (×10⁻⁶)	$\dfrac{\tau_n}{\sqrt{f_c^{'}}}$	$(V_n)_{max}$ (kN)	w_c (mm)	V_n (kN)	v_c	$\dfrac{f_t^{*}}{f_c^{*}}$	φ (deg.)	α (deg.)	V_n (kN)	Vecchio and Collins	Mechanism analysis
A4	31.2	1510	42.4	590	0.317	149.6	0.022	73.9	0.638	0.012	70.2	73.7	40.9	0.574	1.038
A8	36.2	1540	63.2	699	0.438	173.9	0.016	82.2	0.629	0.014	69.1	72.8	49.5	0.769	1.278
A13	31.8	1551	61.0	569	0.450	152.9	0.014	78.2	0.640	0.016	67.3	71.3	48.2	0.779	1.265
A19	37.4	1514	73.4	650	0.500	179.4	0.035	81.5	0.624	0.017	67.0	71.1	55.8	0.901	1.315
S4	34.8	2130	46.1	520	0.325	167.0	0.043	72.5	0.683	0.012	70.1	73.6	49.2	0.636	0.937
S8	29.9	1841	61.2	550	0.466	143.6	0.052	67.1	0.672	0.015	68.0	71.9	46.0	0.913	1.331
S13	36.0	1824	68.1	700	0.473	172.8	0.032	79.4	0.656	0.016	67.5	71.5	55.1	0.858	1.236
S19	33.0	1772	76.6	620	0.555	158.3	0.025	78.3	0.658	0.018	66.1	70.4	54.0	0.978	1.417
N4	25.8	2157	40.8	440	0.335	123.8	0.033	64.7	0.711	0.014	68.9	72.6	40.2	0.631	1.014
N8	29.6	2233	67.0	543	0.513	135.9	0.048	67.5	0.702	0.016	67.6	71.6	48.3	0.991	1.386
N13	27.4	2253	72.2	520	0.575	131.5	0.092	60.1	0.709	0.018	65.8	70.3	48.8	1.201	1.481
N19	36.2	2273	93.4	619	0.646	148.8	0.152	64.3	0.685	0.018	66.1	70.5	61.7	1.452	1.513
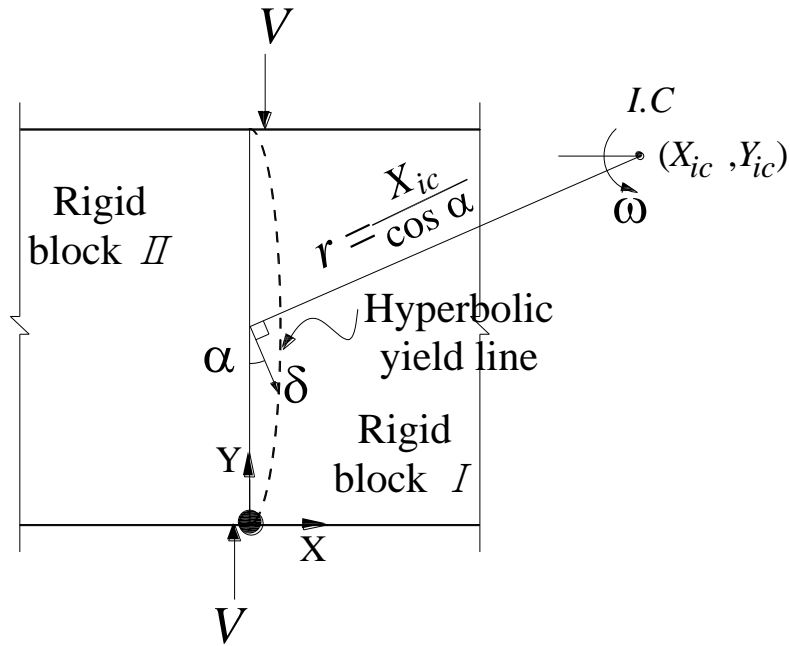
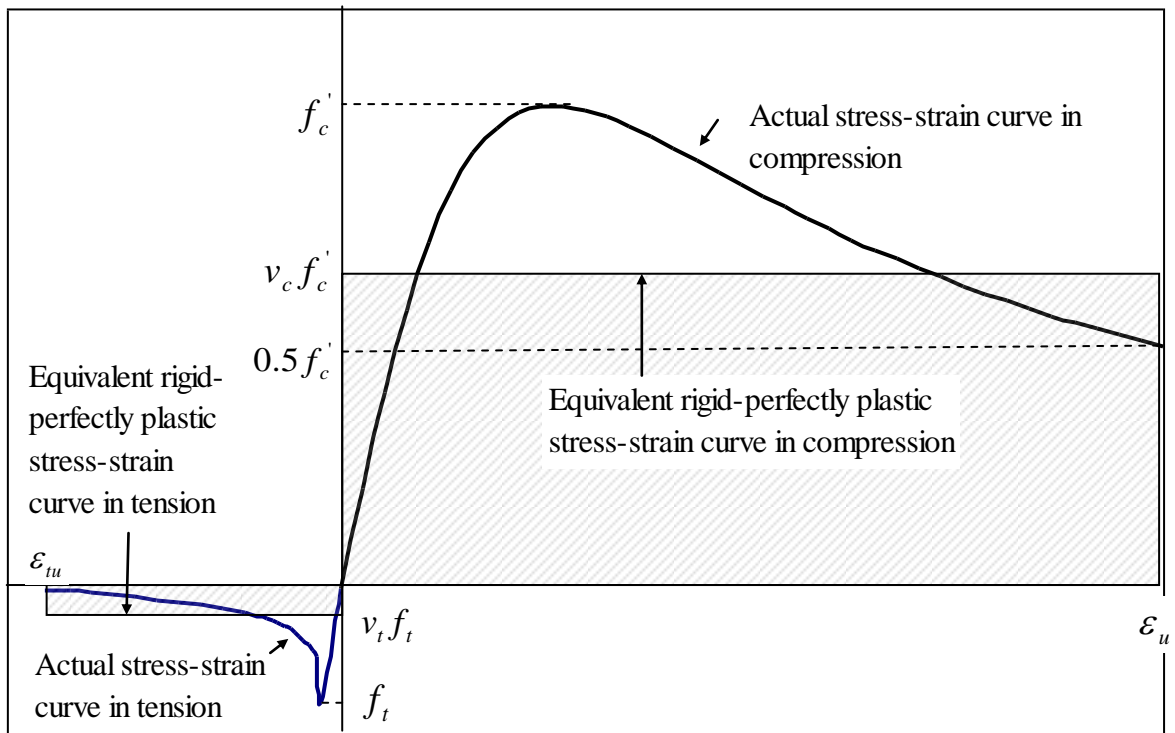**Fig. 1–Idealized failure plane of monolithic concrete joints.**

Fig. 2–Equivalent rigid-perfectly plastic stress-strain curve of concrete.
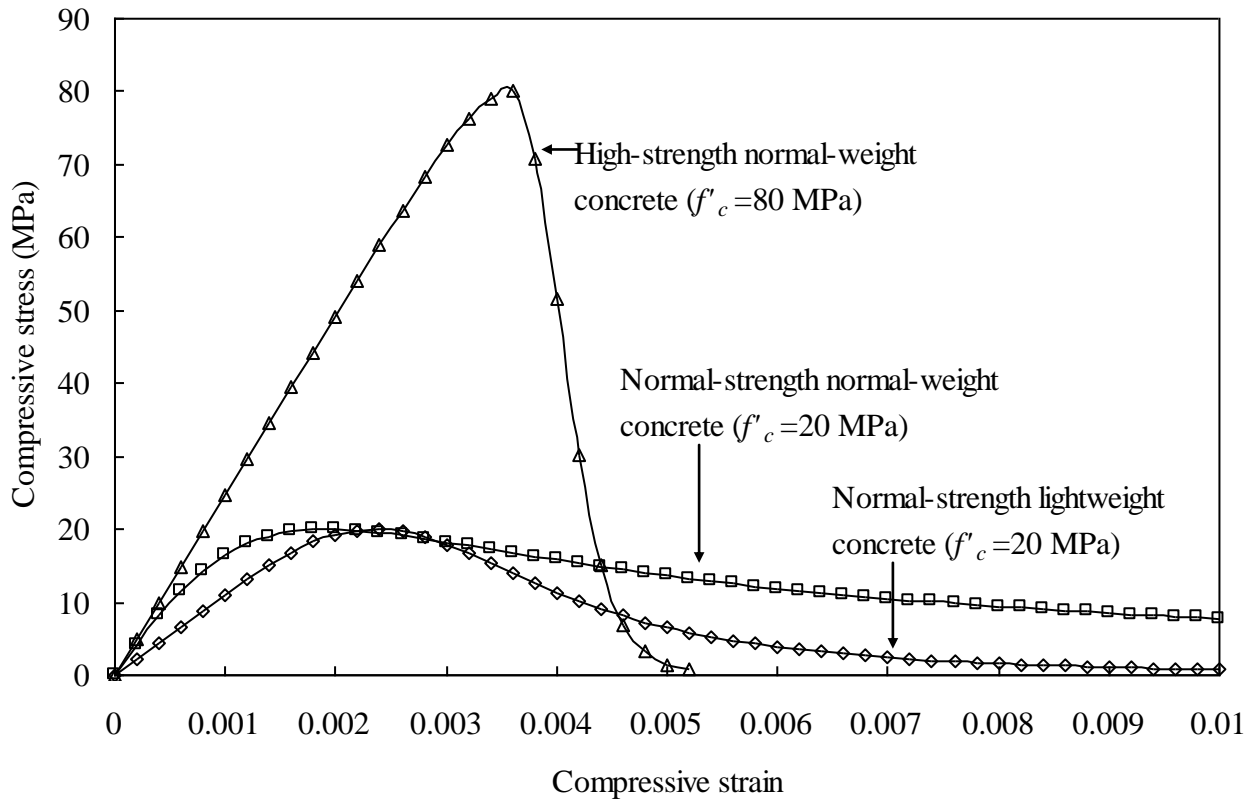
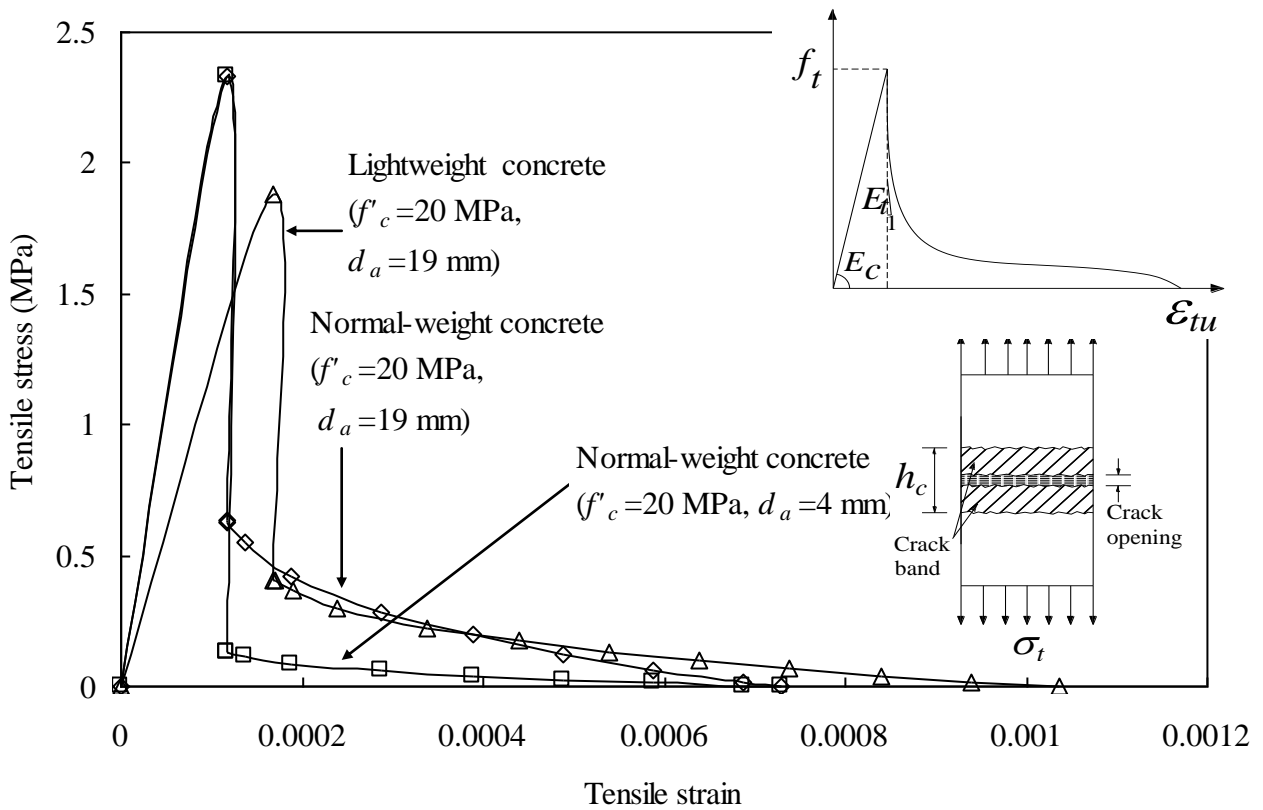**Fig. 3–Typical compressive stress-strain curves of concrete generalized by Eq. (12).**

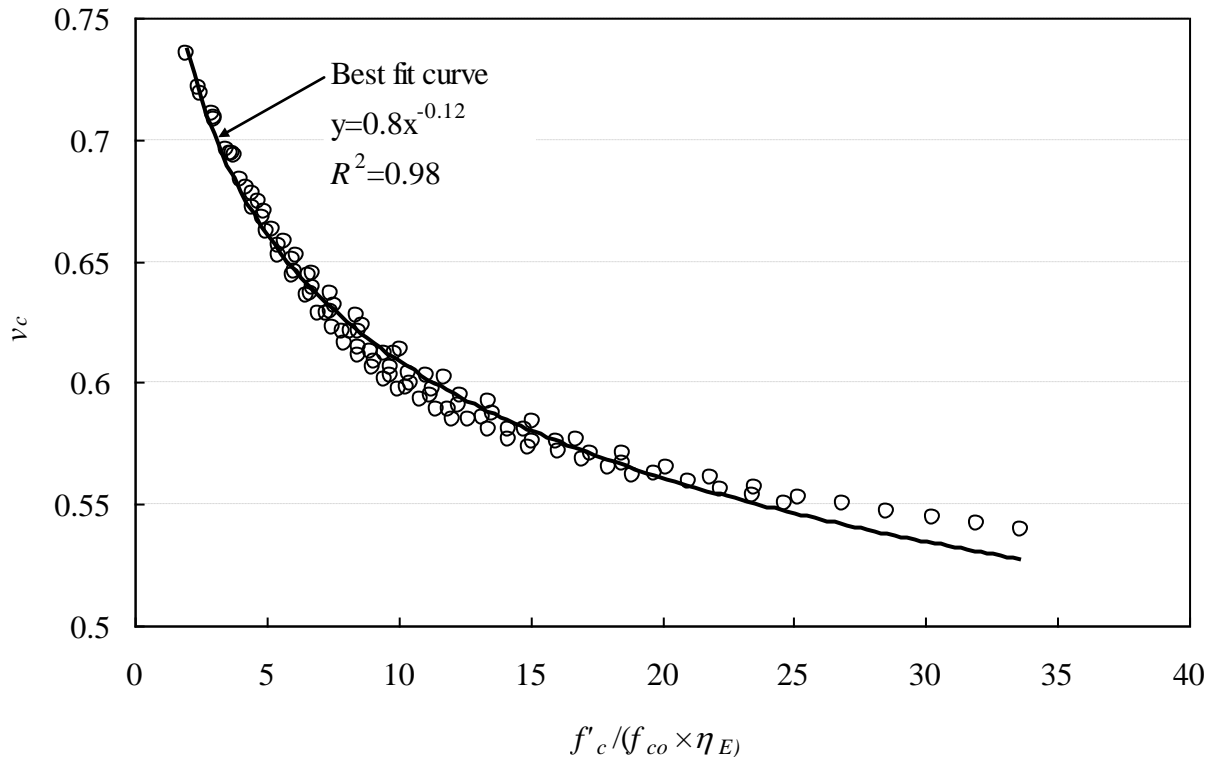**Fig. 4–Typical tensile stress-strain curves of concrete generalized by Eq. (16)**
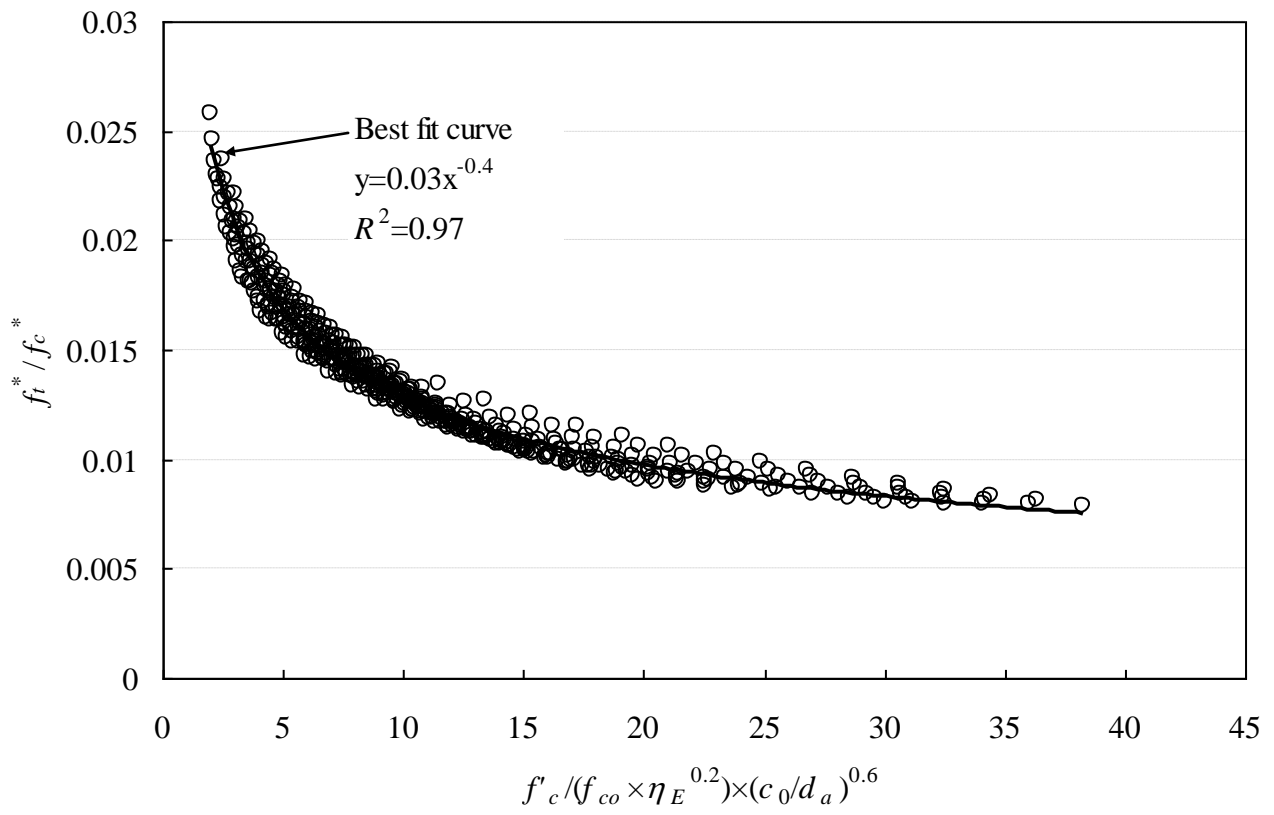
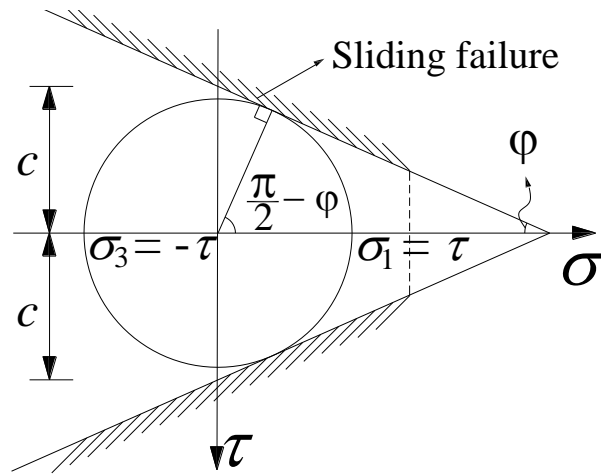**Fig. 5–Regression analysis for** v_c

Fig. 6–Regression analysis for f_t^* / f_c^*
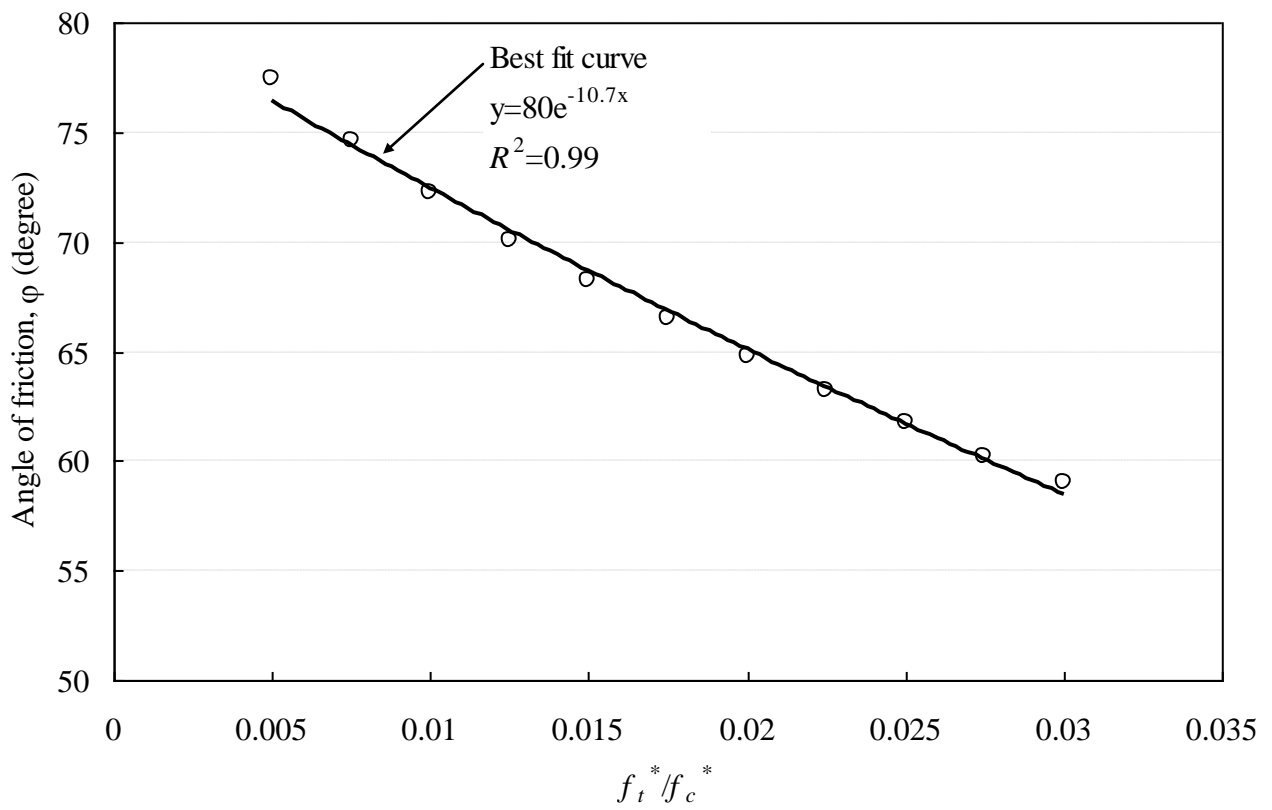
27

Fig. 7–Mohr's circle for sliding failure under pure shear.

Best fit curve
$y=80e^{-10.7x}$
$R^2=0.99$

Angle of friction, φ (degree)

f_t^* / f_c^*
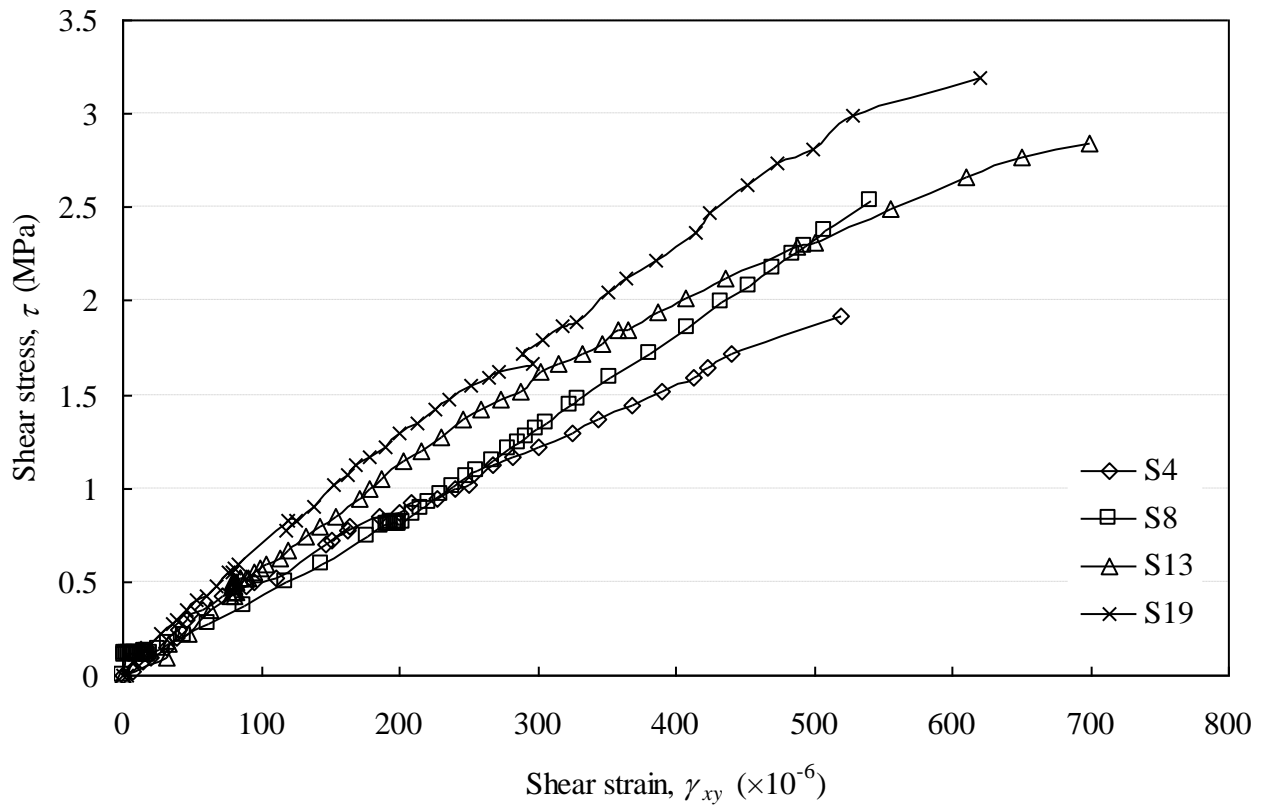
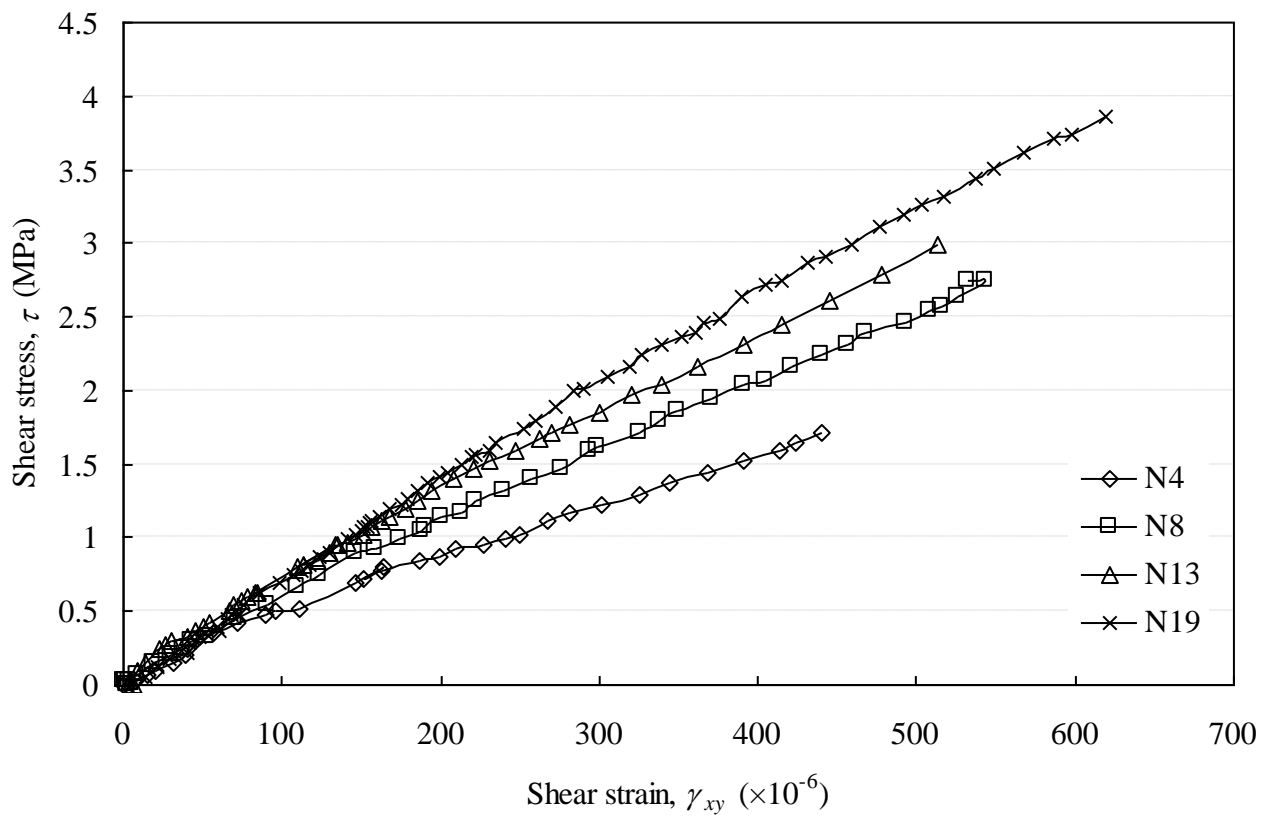**Fig. 8–Relation of f_t^* / f_c^* and φ**
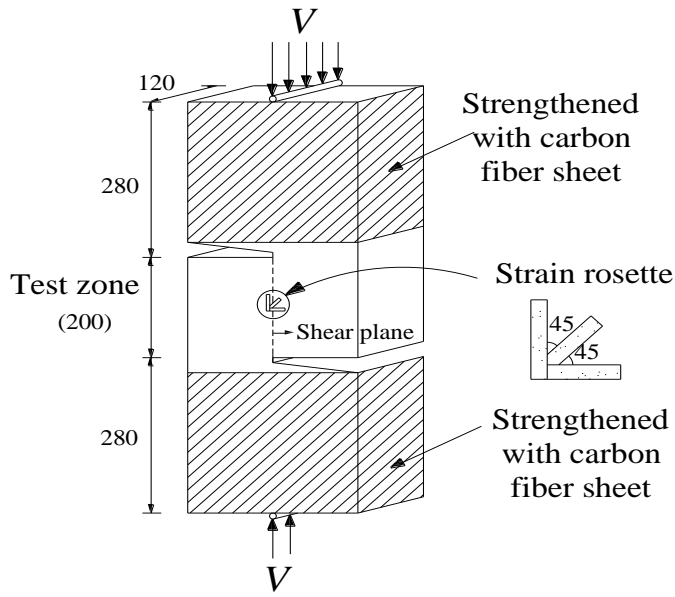
Fig. 9–Details of push-off specimen tested (All dimensions are in mm).
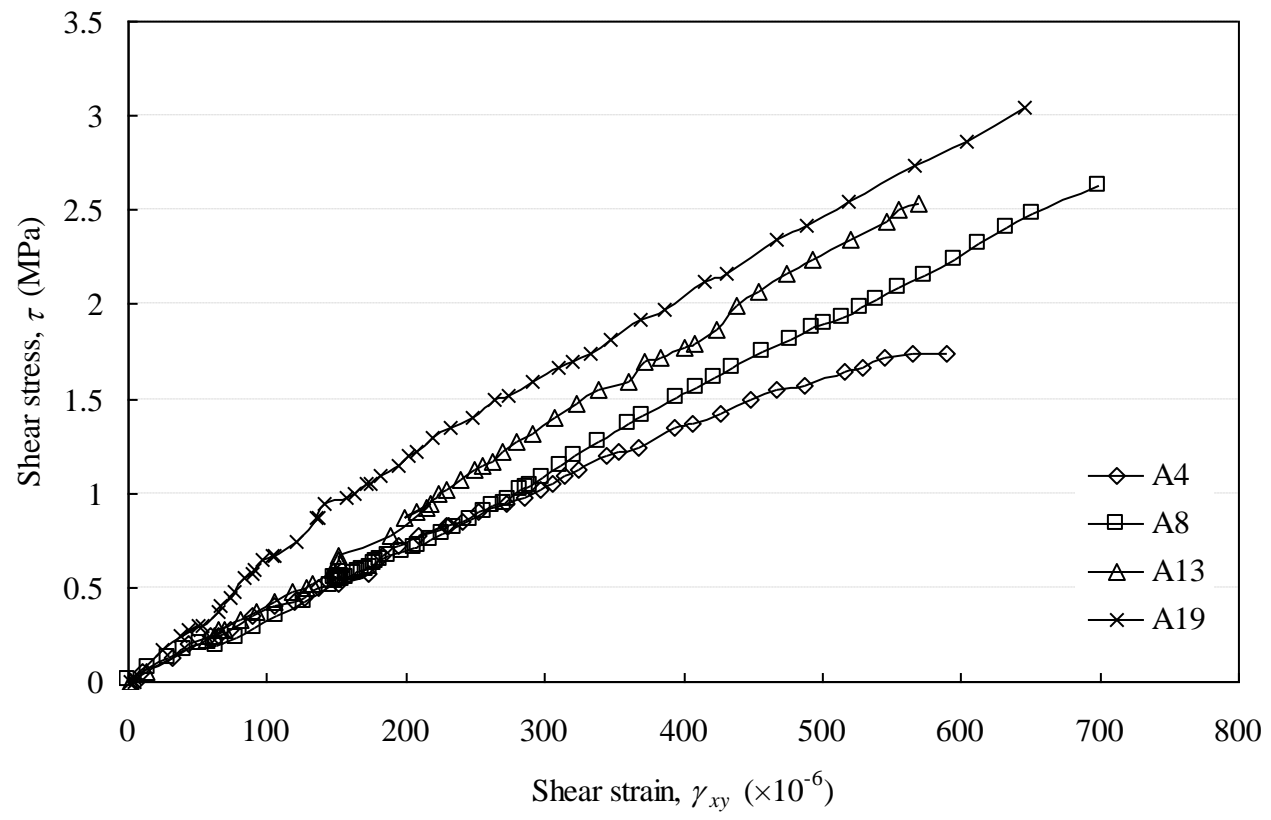
(a) ALWC

(b) SLWC

(c) NWC

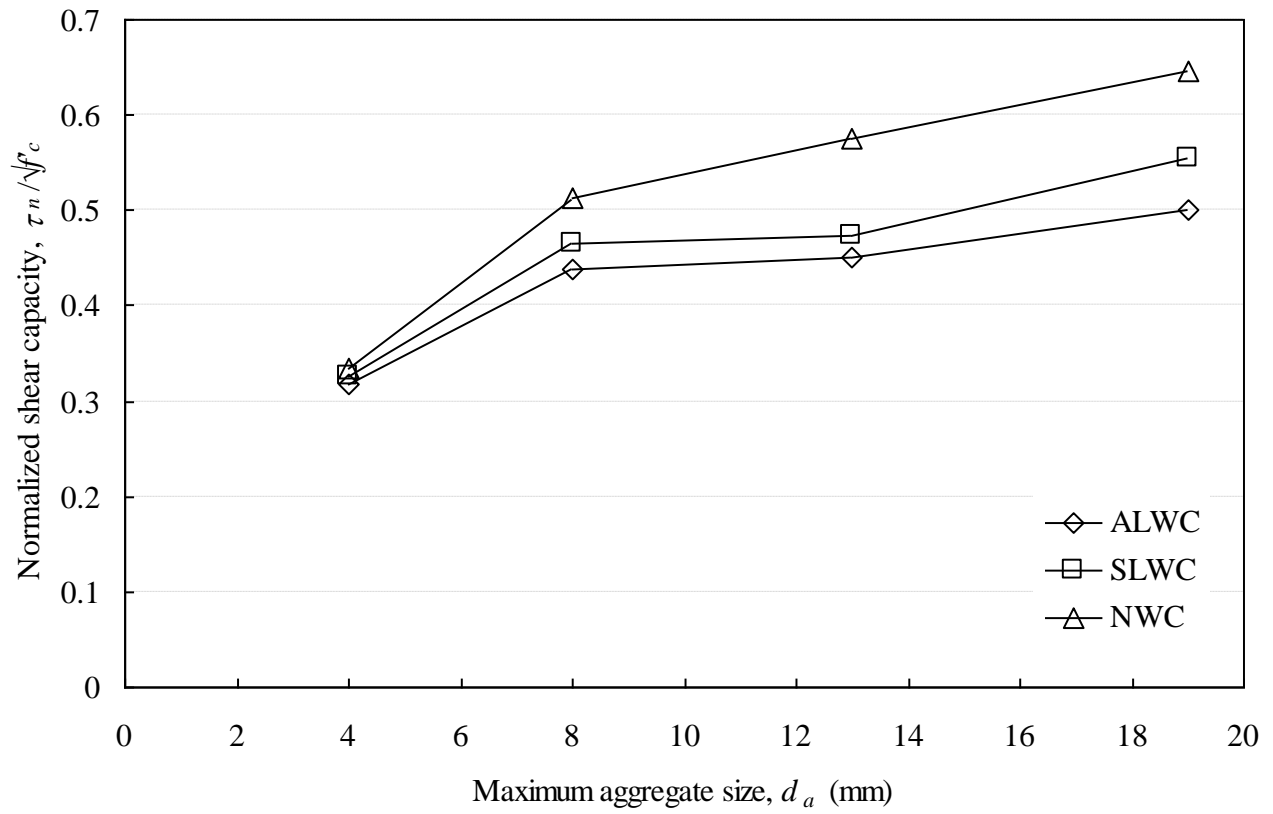**Fig. 10– Shear stress versus shear strain in shear plane of push-off specimens tested.**

Fig. 11 – $\tau_n / \sqrt{f_c^{'}}$ **versus** d_a **.**